

TCAD simulation for transition metal dichalcogenide channel Tunnel FETs consistent with *ab-initio* based NEGF calculation

Hidehiro Asai

Device Technology Research Institute
National Institute of Advanced
Industrial Science and Technology
Tsukuba, Japan
hd-asai@aist.go.jp

Tatsuya Kuroda

Graduate School of Engineering
Osaka University
Suita, Japan
kuroda@si.eei.eng.osaka-u.ac.jp

Koich Fukuda

Device Technology Research Institute
National Institute of Advanced
Industrial Science and Technology
Tsukuba, Japan
fukuda.koichi@aist.go.jp

Junichi Hattori

Device Technology Research Institute
National Institute of Advanced
Industrial Science and Technology
Tsukuba, Japan
j.hattori@aist.go.jp

Tsutomu Ikegami

National Institute of Advanced
Industrial Science and Technology
Tsukuba, Japan
t-ikegami@aist.go.jp

Nobuya Mori

Graduate School of Engineering
Osaka University
Suita, Japan
mori@si.eei.eng.osaka-u.ac.jp

Abstract—We perform TCAD simulation for TMDC channel TFETs with the material parameters considering *ab initio* band structure. By using the WKB-based non-local band-to-band tunneling (BTBT) model with the above parameters, we find that the current voltage characteristics of the TFETs are in good agreement with those obtained by microscopic NEGF calculation. Based on this approach, we also investigate the dependence of tunnel leakage current on the gate length. Our simulation method paves the way for reliable macroscopic device simulations for TMDC channel TFET.

Keywords—TMDC channel TFET, TCAD simulation, NEGF simulation

I. INTRODUCTION

Atomically thin transition metal dichalcogenides (TMDCs) such as MoS₂ and WS₂ are promising candidates as channel material for high performance transistors because of their atomically flat structure and excellent electrostatic controllability [1]. In particular, abrupt van der Waals interface and atomically thin structure will be strong advantage for designing tunnel transistor (TFET) having ultra short tunnel distance (i.e. high ON current). Moreover, wide variety of TMDC materials allows us to design high performance TFET by band engineering approach. Therefore, TMDC based TFETs have been extensively studied [2-6] so far. At the same time, for the design of such novel TFETs, modeling of TMDC devices for technology computer aided design (TCAD) simulation is strongly required. However, the band structures of TMDC materials drastically change with the number of stacking layers. Thus, the precise device modeling based on *ab initio* band structure becomes also crucial for the TCAD simulation. In this paper, we perform TCAD simulation for TMDC TFETs with parameter tuning considering *ab initio* band structure, and show the current-voltage

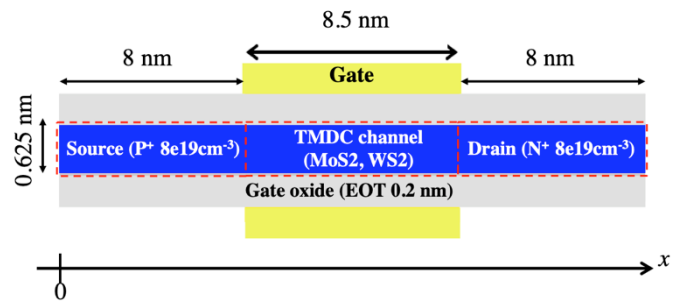


Fig. 1: Schematic figure of N-type TMDC channel TFET.

characteristics which reproduce well those of nonequilibrium Green function (NEGF) calculation.

II. MODEL & METHOD

In this paper, for the comparison between TCAD simulations and NEGF simulations, we considered simple monolayer N-type TFETs as shown in Fig. 1. The dimensions and the dopant concentrations of the TFETs are set to the same values of our previous NEGF calculation [7]. We considered MoS₂ and WS₂ as TMDC channel materials. In our previous NEGF simulation, we employed the three-band nearest-neighbor TB approximation of which considers three atomic d-orbitals of the transition metal atoms [8]. The TB parameters are extracted from the first-principles calculation using the Vienna *ab initio* simulation package VASP [9,10]. In the present paper, we utilized same band parameters for adjusting the band profile and the ON current of the TFET.

We used our homemade TCAD simulator named Impulse TCAD [11]. In order to calculate the tunneling current of the TFETs, we implemented non-local band-to-band tunnel (BTBT) model [12-14] into Impulse

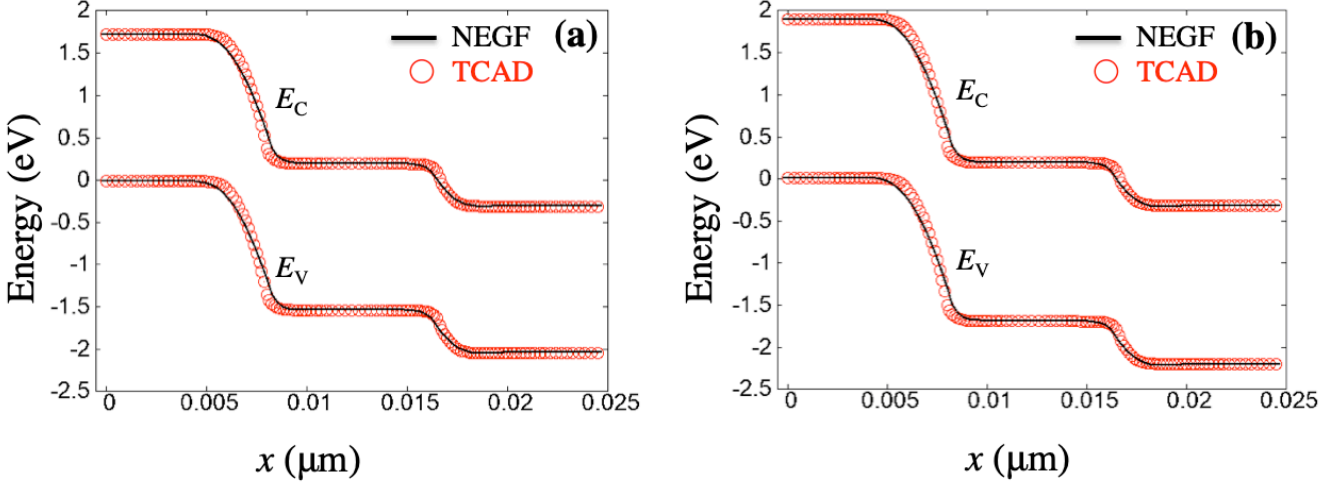


Fig. 2: Conduction and valence band profiles along the source-to-drain direction for (a) MoS2 channel and (b) WS2 channel TFET. The solid lines and the open circles indicate the results of NEGF and TCAD simulations, respectively.

TCAD. The tunneling paths are searched by tracing the energy surface along the steepest gradient direction. The generation rate due to the tunneling G_{BTBT} is calculated along this one-dimensional path. In order to consider the effect of non-uniform electric field along the path (from $x = 0$ to $x = l$), we calculate G_{BTBT} based on WKB method with Kane's relation [15,16],

$$G_{\text{BTBT}} = \frac{e}{36\hbar} E_t \left(\int_0^l \frac{dx}{\kappa} \right)^{-1} \left[1 - \exp \left(-k_m^2 \int_0^l \frac{dx}{\kappa} \right) \right] \times \exp \left(-2 \int_0^l \kappa dx \right) [f_p(\epsilon) - f_n(\epsilon)],$$

$$f_n(\epsilon) = \frac{1}{1 + \exp \left(\frac{\epsilon - E_{\text{fn}}}{k_B T} \right)}, \quad f_p(\epsilon) = \frac{1}{1 + \exp \left(\frac{\epsilon - E_{\text{fp}}}{k_B T} \right)}.$$

Here, κ is the imaginary wave vector along the tunneling path, k_m is the maximum wave vector transverse to the path. E_t is the electric field for tunneling area, and we take the average of the field at the start and the end of the tunneling path. f_n and f_p are Fermi-Dirac distribution for tunneling energy ϵ . E_{fn} and E_{fp} are the quasi Fermi level for the conduction band side and the valence band side, respectively.

III. RESULTS

Firstly, in order to reproduce the potential profile in our previous NEGF calculation, we set the effective density of states for conduction band N_c and valence band N_v of the TMDC material. Figs. 2 (a) and (b) show the calculated conduction and valence band profiles along the source-to-drain direction for MoS2 and WS2 TFETs at $V_{\text{GS}} = 0\text{V}$. Here, we adjusted N_c and N_v so that these parameters are consistent with effective masses calculated by VASP. In both figures, TCAD

simulations reproduce well the band profiles of the NEGF simulations.

Then, we set tunneling mass parameters for WKB model and calculated I_D - V_{GS} curve of the TMDC TFETs. Here, we adjusted the tunneling mass by multiplying constant value to the effective masses calculated by VASP, and we chose 0.925 for both MoS2 and WS2 channel TFETs. Figure 3 shows the I_D - V_{GS} curves for MoS2 and WS2 channel TFETs, respectively. The calculated I_D - V_{GS} curves for both TFETs agree well with those of NEGF calculation. Figs. 4 (a) and (b) show the distribution of the BTBT generation rate in the MoS2 TFET for $V_{\text{GS}} = 0.15$ and 0.3 V. The generation rate in the source region indicates the generation of electrons, while the rate in the channel and the drain regions indicates the generation of holes. As shown in this figure, source to channel tunneling, which contributes to the ON current, occurs in high voltage condition (V_{GS}

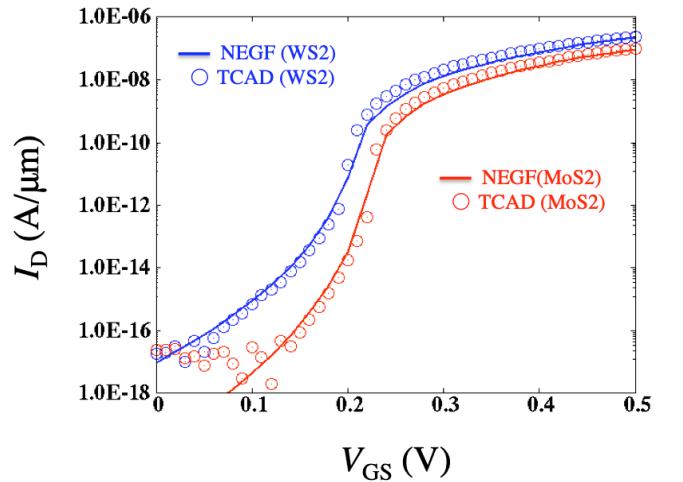


Fig. 3: I_D - V_{GS} curve of TMDC channel TFETs. The solid lines and the open circles indicate the results of NEGF and TCAD simulations, respectively.

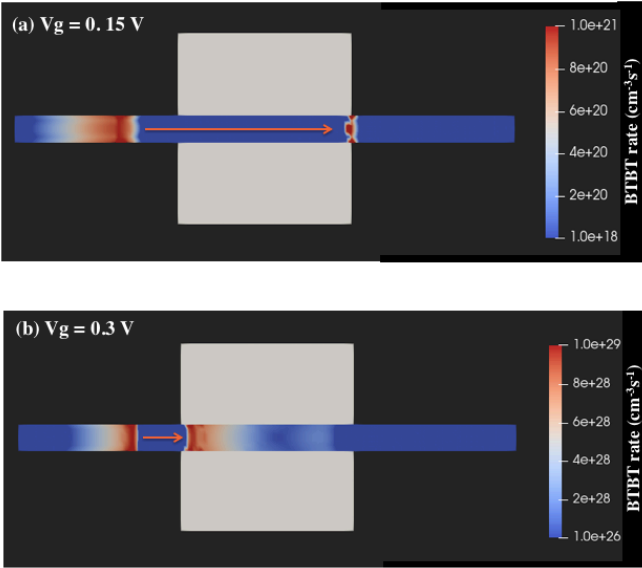


Fig. 4: The distribution of BTBT generation rate in MoS2 channel TFETs for (a) $V_{GS} = 0.15$ V, and (b) $V_{GS} = 0.3$ V.

= 0.3 V). Meanwhile source-to-drain tunneling, which contributes to the OFF-leak current, occurs in low voltage condition ($V_{GS} = 0.15$ V). Our TCAD simulation reproduces well both tunneling processes. The key parameters for both MoS2 and WS2 channel TFETs optimized in this study are listed in Table 1.

Finally, using the above parameters, we performed TCAD simulation for the TFET whose gate length L_G is much larger than that in the NEGF simulation. Figs. 5 (a) and (b) show I_D - V_{GS} curve of MoS2 and WS2 channel TFETs for $L_G = 8.5$ -40 nm, respectively. The tunneling mass of WS2 is smaller than that of MoS2, because of which both the ON and OFF currents of the WS2 TFETs are larger than those of the MoS2 TFETs. However, as the gate length increases, only the OFF

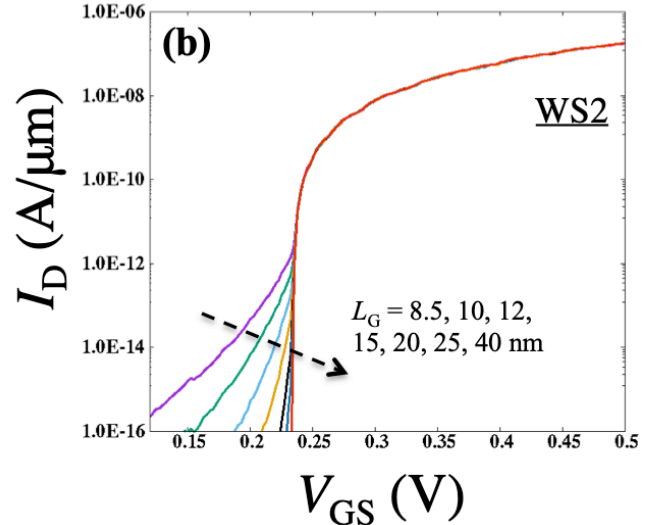
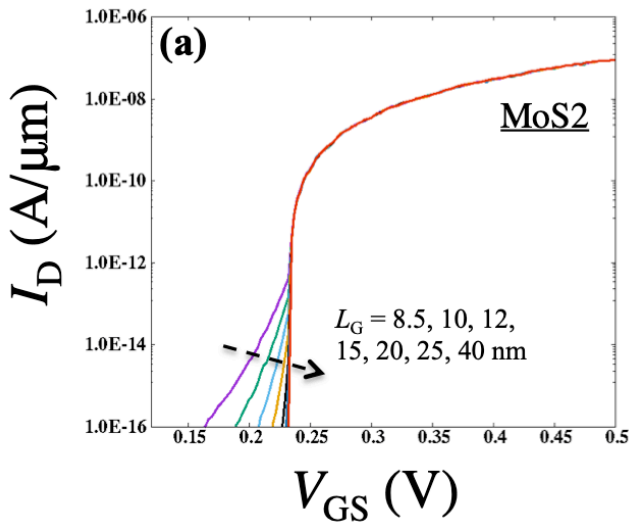


Fig. 5: I_D - V_{GS} curve of (a) MoS2, and (b) WS2 channel TFETs for $L_G = 8.5$ -40 nm.

	MoS2	WS2
N_c	$6.73 \text{ e}19 \text{ cm}^{-3}$	$4 \text{ e}19 \text{ cm}^{-3}$
N_v	$9.51 \text{ e}19 \text{ cm}^{-3}$	$5.94 \text{ e}19 \text{ cm}^{-3}$
m_c	$0.446 m_e$	$0.301 m_e$
m_v	$0.561 m_e$	$0.391 m_e$

m_e : electron mass

Table: The optimized key parameters for both MoS2 and WS2 channel TFETs.

leak current decreases, and it becomes negligibly small for large L_G . Fig. 6 shows I_{ON}/I_{OFF} ratio at an operating voltage $V_D = 0.15$ V as a function of L_G . Here, I_{ON} is defined as I_D at $V_{GS} - V_{th} = 0.15$ V, and the threshold voltages V_{th} is the voltage at which I_D reaches 10^{-13} A/ μm . The degradation of the I_{ON}/I_{OFF} ratio due to the OFF-leak current is considerably large in the WS2 TFETs compared with that in the MoS2 TFETs. However, this degradation is suppressed for the devices having large gate length ($L_G > 15$ nm).

IV. CONCLUSION

We performed TCAD simulations for TMDC channel TFETs. By adjusting the parameters for effective density of states and the tunnel masses in a way that is consistent with *ab initio* band structure, we succeeded to reproduce well the current voltage characteristics of the TFETs by NEGF calculation. We also investigated the dependence of I - V characteristics of the TFETs on the gate length, and discussed the short channel effect in the TMDC channel TFETs. The simulation method presented in this paper is simple, but is a useful approach to achieve reliable design of novel TFETs based on *ab initio* calculations.

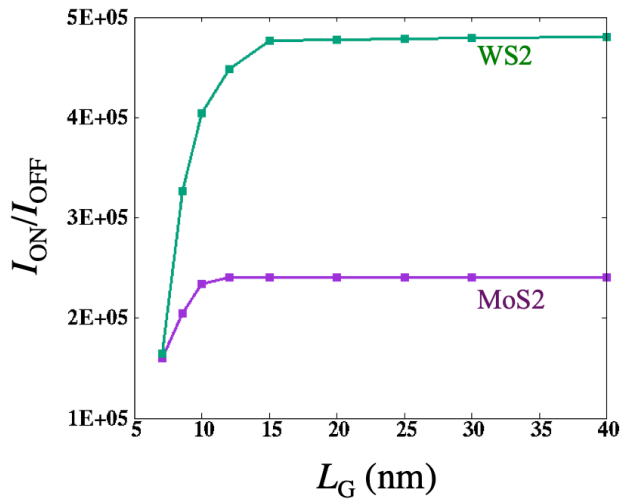


Fig. 6: I_{ON}/I_{OFF} ratio of the MoS2 and WS2 channel TFETs as a function of L_G .

ACKNOWLEDGEMENT

This work was supported by JST CREST (JPMJCR16F3).

REFERENCES

- [1] A. Rai *et al.*, Crystals **8**, 316 (2018).
- [2] D. Sarkar *et al.*, Nature **526**, 91 (2015).
- [3] W. Cao *et al.*, IEDM Tech. Dig. **305** (2015).
- [4] A. Nourbakhsh *et al.*, Nano Lett. **16**, 1359 (2016).
- [5] J. He *et al.*, Adv. Electron. Mater. **4**, 1800207 (2018).
- [6] T. Irisawa *et al.*, Jpn. J. Appl. Phys. **59**, SGGH05 (2020)
- [7] T. Kuroda and N. Mori, Jpn. J. Appl. Phys. **57**, 04FP03 (2018).
- [8] G. B. Liu, *et al.*, Phys. Rev. B **88**, 085433 (2013).
- [9] G. Kresse and J. Hafner, Phys. Rev. B **47**, 558(R) (1993).
- [10] G. Kresse and J. Furthmüller, Phys. Rev. B **54**, 11169 (1996).
- [11] T. Ikegami *et al.*, J. Comput. Electron. **18**, 534 (2019).
- [12] K. Fukuda *et al.*, Jpn. J. Appl. Phys. **114**, 144512 (2013).
- [13] K. Fukuda *et al.*, Jpn. J. Appl. Phys. **56**, 04CD04 (2017)
- [14] H. Asai *et al.*, AIP Advances **8**, 095103 (2018).
- [15] E. O. Kane, J. Appl. Phys. **32**, 83 (1961).
- [16] Sentaurus Device User Guide. Version K-2015.06, June 2015, Synopsys.